Optics Communications 286 (2013) 192–196

Contents lists available at SciVerse ScienceDirect

Optics Communications

journal homepage: www.elsevier.com/locate/optcom

Improving slow light effect in photonic crystal line defect waveguide by using eye-shaped scatterers

Yong Wan [a,b,*], Kai Fu [a], Changhong Li [c], Maojin Yun [a]

[a] College of Physics Science, Qingdao University, Qingdao 266071, PR China
[b] Institute of Multifunctional Materials (IMM), Qingdao University, Qingdao 266071, PR China
[c] College of Automation, Qingdao University, Qingdao 266071, PR China

ARTICLE INFO

Article history:
Received 31 July 2012
Received in revised form
5 September 2012
Accepted 8 September 2012
Available online 24 September 2012

Keywords:
Scatterers
Photonic crystal
Waveguide
Slow light
Group index

ABSTRACT

Eye-shaped scatterers are adopted into a photonic crystal waveguide (PCW) in two ways: (1) slow light with wide bands and group index n_g from 14.1 to 32.8 can be generated by simply replacing the first and second rows of air holes adjacent to the linear defect with eye-shaped scatterer and (2) slow light with wide bands of n_g from 36.5 to 287.5 are achieved by substituting all air holes with eye-shaped scatterers. More simulation results show that the latter method can achieve slow light with low dispersion at large n_g, and near zero dispersion structures by adjusting the lattice parameter a and parameter e (e is inversely related to the ratio of the radius of the minor axis c to that of the major axis b).

1. Introduction

Slow light with a small group velocity v_g is found useful in compact optical delay lines and optical buffers. It can be observed close to the Brillouin zone edge in a photonic crystal waveguide (PCW) by using the photonic bandgap of photonic crystal [1–3]. Photonic nanostructures can also generate on-chip slow light at room temperature and achieve any slow light operating wavelength by correctly, scaling the structural parameters of the photonic crystal with less loss [4–6]. There are two basic kinds of PCWs for slow light: line defects waveguide and coupled resonator waveguide. Unfortunately, both of them encounter the same problem: a low group velocity may accompany a high group velocity dispersion (GVD), which may offset most of the advantages of operation in the slow light region and severely limit the width of flat band [7].

Aimed to achieve wide band and low GVD slow light with high group index n_g, many successful researches have been conducted. For line defect waveguides, the improvements include reducing the waveguide width [8], changing the PCW parameters by shifting anticrossing points [9],using slotted photonic crystal waveguides [10,11], adjusting the diameters of the holes [12–14], introducing a hetero-group velocity waveguide [15,16], shifting the first and second rows of air holes or shifting lattice along the waveguide defects [17–19], infiltrating microfluid into the air holes [20,21] or using a technique based on selective liquid infiltrations to precisely and reversibly change the structures [22], etc. For coupled resonator waveguide, the improvements include chirping airhole diameters only or both radius of holes in the center row and radius of those besides the waveguide [23,24], shifting the shear along the defect interface over a distance of one crystal period [25], using a chain of weakly coupled cavities [26], changing the radius of defect rods and the position of the rods nearby the missing rods simultaneously [27], integrating side-coupled cavities in photonic crystal waveguide [28], etc. Some existing researches also combined two kinds of PCWs to achieve low group velocity and low dispersion, such as adding high-Q multicavities or single quantum nanocavity side-coupled to a line defect photonic crystal waveguide [29,30].

Among the above papers, experimental ones are minority [4,6,10,12,19,22,29], while most of them are theoretical research and they neglected the acceptable tolerance of fabrication. Another phenomenon is that most of these methods focus on the variation of periodic arrays of scatterers, and the scatterers are usually cylindrical. Only a few research changed the shapes of scatterers [31].

In our previous study, we at first introduced eye-shaped scatterers into PCWs instead of cylinder holes on silicon wafer. It is found that the widths of bandgaps and their positions can be effectively adjusted by changing parameters of eye-shaped scatterers [32]. In this paper, according to the PCW1 waveguide, we adopted eye-shaped scatterers into PCWs in two ways: (1) wide

* Corresponding author at: Qingdao University, College of Physics Science, No 308 Ningxia RoadChina, Qingdao 266071, China.
E-mail address: wanyong03@yahoo.com.cn (Y. Wan).

0030-4018/$ - see front matter © 2012 Elsevier B.V. All rights reserved.
http://dx.doi.org/10.1016/j.optcom.2012.09.025

bands from 23.2 nm to 70.4 nm for slow light with n_g from 14.1 to 32.8 can be generated by replacing the first and second rows of air holes and (2) wide bands for slow light are achieved for n_g up to 287.5 by substituting all air holes with eye-shaped scatterers. Moreover, we obtained flat slow light with bandwidths from 3.2 nm to 30.0 nm, where the group index variation is within a range of 10%. These results show that the latter way can achieve a wideband slow-light PCW with low dispersion simultaneously.

2. Simulation

Fig. 1(a) is a schematic diagram of PCW structure with the first and second rows of air holes adjacent to the line defect replaced by eye-shaped scatterers; Fig. 1(b) is a schematic diagram of PCW structure with all the air holes replaced by eye-shaped scatterers. The PCWs are triangular lattice structures on silicon wafer ($n_{Si}=3.46$) with same lattice parameter $a=1$ μm (since n_g is not determined by it) and with line defect at the center. Parameters b and c stand for the radius of the major axis and that of the minor axis of the eye-shaped scatterer, respectively. Define parameter $e=1-c/b$, with range from 0 to 1. This parameter describes the degree of deviation of the eye-shape from a circle, and it is chosen because the ratio of b to c is more relevant to the shape of the eye-shape and thus the optical properties of the scatterers than the value of either b or c.

In the supercell calculation, based on the plane-wave expansion (PWE) method, we selected the number of plane waves in each axis as 32 and the eigenvalue tolerance as 10^{-8} for the sufficient calculation precision.

The well-known relationship between the dispersion and n_g can be given as Eq.(1):

$$n_g = \frac{c}{v_g} = c\frac{dk}{d\omega} = n_{eff} + \omega\frac{dn_{eff}}{d\omega} \tag{1}$$

where n_{eff} is the effective index and ω is the central angle frequency of the incident pulse. Here n_{eff} and ω can be substituted by the propagation constant $k=2\pi n_{eff}/\lambda$, where λ is the operating wavelength, and f the normalized frequency, $f=\omega a/2\pi c$. For slow light, $n_g \gg n_{eff}$, Eq.(2) can be deduced from Eq. (1), based on which we can obtain low-dispersion (n_g is nearly a constant) slow light in specific frequency regions where f varies linearly with k:

$$n_g = \frac{a}{2\pi}\frac{dk}{df} \tag{2}$$

To obtain wideband and flat slow light with large n_g simultaneously, we simply varied parameters a, b and e. Fig. 2 shows the relationship between f and k for the TE even mode while parameters b and e are adjusted for optimization. The linear region of each curve corresponds to a flatband slow-light region with a specific n_g determined by its slope. Fig. 2(a) is the relationship between f and k for the structure in Fig. 1(a); Fig. 2(b) is the relationship between f and k for the structure in Fig. 1(b). In each figure, the curve corresponding to PCW1 waveguide ($e=0$) is provided for comparison.

In order to evaluate the low-dispersion bandwidth of the slow light, most researches selected a bandwidth criterion where n_g varies within a 10% range. Fig. 3 shows the calculated n_g as a function of f. Fig. 3(a) shows the relationship between n_g and f for the structure in Fig. 1(a), in which bandwidths of 70.4, 48.9, 31.5, and 23.2 nm were obtained for nominal group indices of 14.1, 17.4, 24.2, and 32.8, respectively; Fig. 3(b) shows the relationship between n_g and f for the structure in Fig. 1(b), in which bandwidths of 30.0, 22.5, 14.3, 7.1, and 3.2 nm were obtained for nominal group indices of 36.5, 56.1, 96.7, 157.5, and 287.5, respectively.

The dispersion relationship between n_g and f in Fig. 3 is unchanged, so we could enlarge or reduce the PCW structures

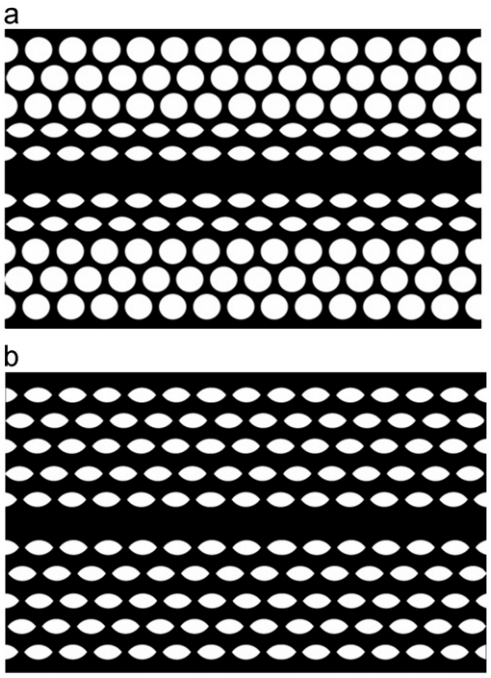

Fig. 1. The schematic diagrams of two types of the PCW structures: (a) a schematic diagram of PCW with the first and second rows of air holes replaced by eye-shaped scatterers; (b) a schematic diagram of PCW with the all of air holes replaced by eye-shaped scatterers.

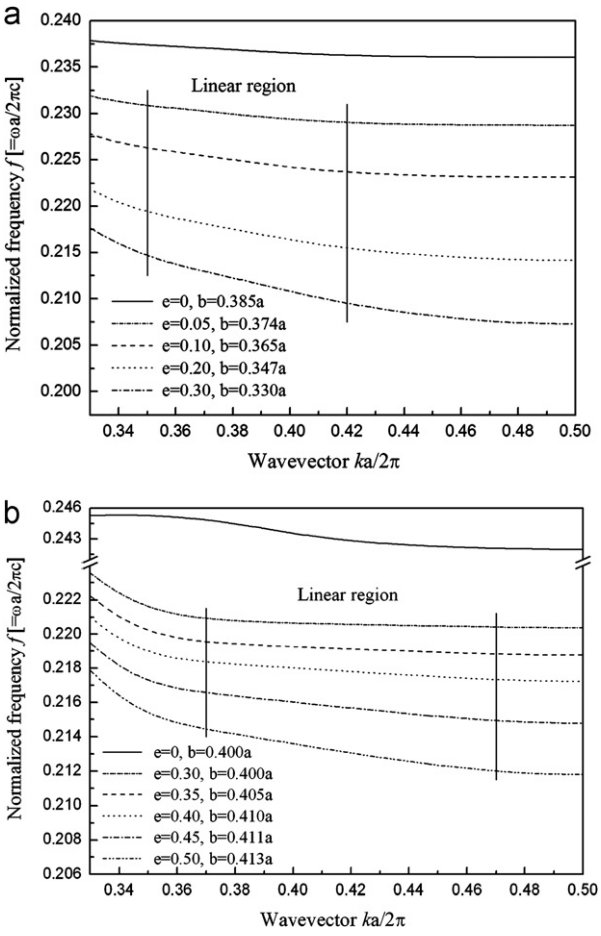

Fig. 2. (a) The relationship of f with k for the Fig. 1(a) structure and (b) The relationship of f with k for the Fig. 1(b) structure.

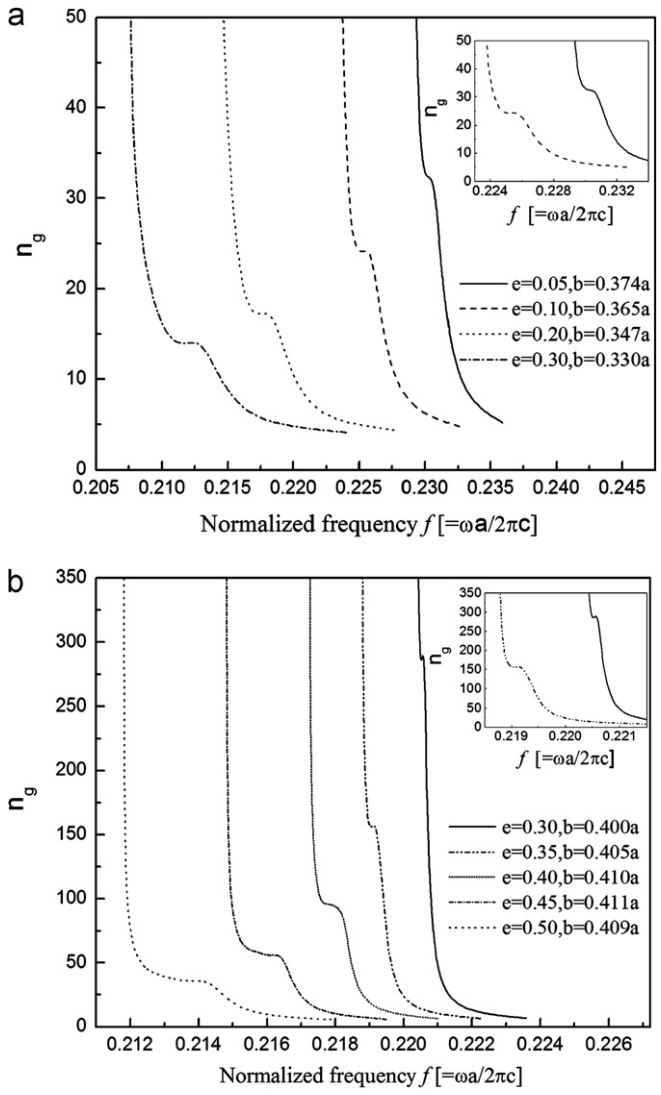

Fig. 3. (a) The relationship between n_g and f for the structure in Fig. 1(a) and Fig. 3 (b) the relationship between n_g and f for the structure in Fig. 1(b).

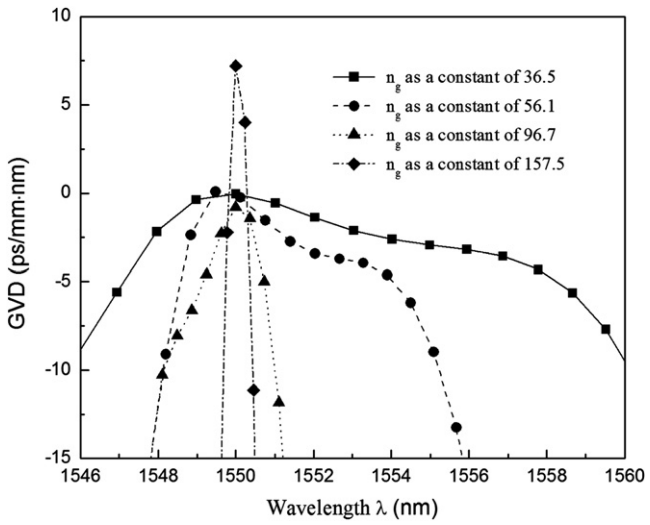

Fig. 4. The GVD as a function of wavelength for the Fig. 1 (b) structure, but the nominal operating wavelength region is around 1550 nm.

Table 1(a)
Group index, bandwidth with different parameters for Fig. 1(a) structure.

e	b	n_g	$\Delta\lambda$ (nm)	$n_g\,\Delta\omega/\omega$
0.05	0.374a	32.8	23.2	0.1763
0.10	0.365a	24.2	31.5	0.1704
0.20	0.347a	17.4	48.9	0.1808
0.3	0.330a	14.1	70.4	0.2089

Table 1(b)
Group index, bandwidth with different parameters for Fig. 1(b) structure.

e	b	n_g	$\Delta\lambda$ (nm)	$n_g\,\Delta\omega/\omega$
0.30	0.400a	287.5	3.2	0.2035
0.35	0.405a	157.5	7.1	0.2439
0.40	0.410a	96.7	14.3	0.2999
0.45	0.411a	56.1	22.5	0.2725
0.50	0.409a	36.5	30.0	0.2304

proportionally, and obtain low dispersion structures with arbitrary operating wavelength of interest by simply adjusting the value of parameter a without renewing the simulation. And we should trim parameter a in a narrow range to get near zero dispersion structure. For operating wavelength $\lambda=1550$ nm, the relationship can be simply summarized as $a=f\lambda$, so parameter a is around 335 nm. For near zero dispersion structures, we will adjust accurately the value of parameter a later. To further illustrate the dispersion property of the flat band with operating wavelength in Fig. 2(b), we defined the GVD parameter D as follows [14].

$$D=\frac{1}{c}\frac{\partial n_g}{\partial\lambda} \tag{3}$$

According to Eq. (3), the PCW structure must have a near-zero GVD if the slope of n_g (λ) is near zero. Fig. 4 shows dispersion curves as a function of wavelength for different n_g when operating wavelength $\lambda=1550$ nm.

3. Results and discussion

For the slow light effect, PCW structure with all air holes replaced by eye-shaped scatterers is better than that with only the first and second rows of air holes replaced by eye-shaped scatterers, as in Fig. 1. To see the simulation results clearly, we transferred the data of Fig. 3(a) and (b) into Table1(a) and Table1 (b). In Table 1(a), the largest n_g is 32.8 with a bandwidth of 23.2 nm. In Table 1(b), the largest n_g is 287.5 with a bandwidth of 3.2 nm. Although in Table 1(a), the largest bandwidth is 70 nm, the value of n_g is only 14.1. Another main performance index for slow light devices is the parameter $n_g\,\Delta\omega/\omega$ which indicates the normalized delay-bandwidth product, and it is proportional to the delay-bandwidth per unit length[33]. For the structure in Fig. 1(a), $n_g\Delta\omega/\omega$ is around 0.18. And for the structure in Fig. 1(b), $n_g\Delta\omega/\omega$ is around 0.24, which is larger than the former and the values reported in other papers as well.

The mechanism of the slow-light effect in the PCW is usually classified into two different aspects, back-scattering and omni-directional reflection. For cylindrical scatterers, the back-scattering is the main reason of dispersion, which can be improved by reducing the waveguide width [7], using slit photonic crystal waveguides [8,9], adjusting the diameters of the holes [10–13], or replacing the first and second rows of air holes by eye-shaped scatterers. However, it will inevitably increase omni-directional reflection with the change of scatterers. The back-scattering can be controlled by varying the eye-shaped parameters b and e. The monotypic eye-shaped scatterers can

also avoid interference between the signal and the back-scattering pulse, and then decrease the omni-directional reflection. All these can make GVD significantly depressed, as shown in Fig. 2.

As mentioned earlier, to obtain near zero dispersion structures, we need to adjust the value of parameter a only slightly according to the bandgap curves [32]. For operating wavelength $\lambda=1550$ nm, we can set $a_1=331.5$ nm for $n_{g1}=36.5$, $a_2=335.0$ nm for $n_{g2}=56.1$, $a_3=337.6$ nm for $n_{g3}=96.7$, $a_4=339.6$ nm for $n_{g4}=157.5$, and $a_1=344.0$ nm for $n_{g5}=287.5$. So parameter a can change in a range from 331 nm to 344 nm.

To see the simulation results for parameter D clearly, we transferred the information of Fig. 4 into Table 2, where all the nominal operating wavelengths were fixed around 1550 nm by setting parameter a to different values according to Eq. (3). Similar to the GVD feature under a small value of n_g, the GVD still stays very low as expected even for a high n_g. Taking $n_g=36.5$ as an example, the GVD stays within ± 3 (ps/mm nm) over 7.4 nm, which has been considered to be a quite low-dispersion region [14]. Even for $n_g=157.5$, the GVD stays within ± 15 (ps/mm nm) over 0.9 nm, which was considerably unattainable in previous models published [14,16].

Though our research consists of only theoretical analysis instead of practical fabrication, we would like to mention the two factors that may affect the slow light in experiment. One is the acceptable tolerance of fabrication and the other is the thickness of waveguide wafer. Fabrication error was simulated with additional simulations with values around the exact value. For instance, in Fig. 5, we chose four values ($+1$ nm, $+0.5$ nm, -0.5 nm and -1 nm) around the exact value of b_3 ($b_3=0.411a_3=138.8$ nm) and ran additional simulations with these four values. The same was applied to h where in Fig. 6 the value of h is $0.7a=235$ nm.

So far the acceptable tolerance of fabrication is ± 20 nm. Taking $n_g=56.1$ as an example, $a=335.0$ nm, according to the optimized parameters listed in Table 1(b), we tuned parameters b slightly, the results are shown in Fig. 5. The solid curve corresponds to the ideal

Table 2
Parameter *D* with parameter *a* around 335 nm for different group indices in Fig. 1(b) structure.

n_g	a (nm)	$\lvert D \rvert$ (ps/mm · nm)	$\Delta\lambda$(nm)
36.5	331.5	≤ 3	7.4
56.1	335.0	≤ 5	5.4
96.7	337.6	≤ 10	2.7
157.5	339.6	≤ 15	0.9

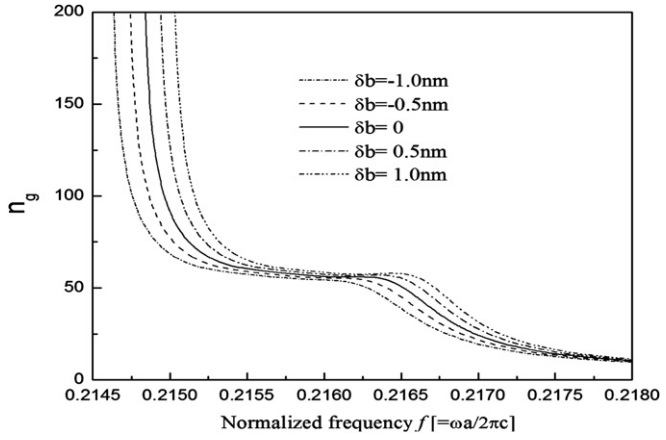

Fig. 5. n_g as a function of normalized frequency with fabrication errors relative to parameter *b* when $n_g=56.1$ as listed in Table 1(b).

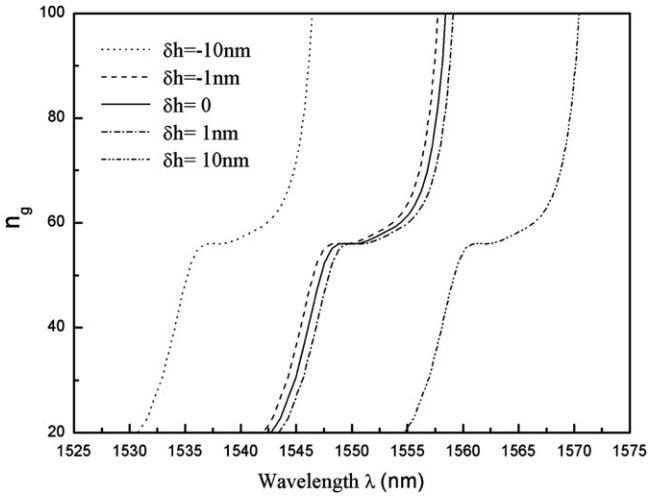

Fig. 6. n_g as a function of wavelength with fabrication errors relative to parameter *h* when $n_g=56.1$ as listed in Table 1(b).

model without any fabrication error. We can see from Fig. 5 that the flat band part of the curve remains almost unchanged around $n_g=56.1$ when the fabrication error is within ± 1 nm, but this precision cannot be achieved with e-beam lithography now.

Fortunately, the PCW structures can be enlarged or reduced proportionally according to the operating wavelength, and the state of art fabrication tolerance (± 20 nm) is sufficient for practical uses of terahertz wave, which corresponds to $a=120$ μm (consider that ± 1 nm of error corresponds to $a=355$ nm), as in our previous research [32]. Hopefully, the fabrication error will continue to decrease with the development of technology.

The result for the thickness of the wafer h is a little more complicated. In the simulation, we controlled the initial value of the thickness at 235 nm (around 0.7* Period). If parameter h is allowed to vary within ± 1 nm, the flattened region and its position are almost unchanged; if parameter h is allowed to vary by ± 10 nm, the flattened region is still unchanged, but its position takes a considerable red-shift with the increase of h, which we can see from Fig. 6. This result is coherent with other research [34].

4. Conclusion

We obtained slow light with bandwidths from 23.2 nm to 70.4 nm (when $a=1$ μm), where the group index variation is within a range of only 10%, and slow light with n_g from 14.1 to 32.8 can be generated by simply replacing the first and second rows of air holes with eye-shaped scatterers. Moreover, we obtained slow light with a flat band for n_g up to 287.5 and bandwidths from 3.2 nm to 30.0 nm by substituting all air holes with eye-shaped scatterers. We also attained near-zero dispersion structures by adjusting the value of parameter a slightly. All these achievements indicate that the latter method enables us to achieve a wideband slow-light PCW with ultralow dispersion simultaneously. In a broad sense, we can attain slow light with a large group index by choosing new scatterers and adjusting their parameters, as well as changing the periodic arrays of scatterers.

Acknowledgments

This work is supported by the National Natural Science Foundation of China (NSFC, 11144007), and the Science Foundation of

Shandong Province (No. BS2012CL012). The Taishan Scholars Program of Shangdong Province is also acknowledged.

References

[1] Z. Shi, R.W. Boyd, D.J. Gauthier, C.C. Dudley, Optics Letters 32 (2007) 915.
[2] T. Baba, Nature Photonics 2 (2008) 465.
[3] T.F. Krauss, Journal of Physics D 40 (2007) 2666.
[4] S. Assefa, S.J. McNab, Y.A. Vlasov, Optics Letters 31 (2006) 745.
[5] A.Yu. Petrov, M. Eich, Applied Physics Letters 85 (2004) 4866.
[6] C. Monat, B. Corcoran, M. Ebnali-Heidari, C. Grillet, B.J. Eggleton, T.P. White, L. O'Faolain, T.F. Krauss., Optics Express 17 (2009) 2944.
[7] R.J.P. Engelen, Y. Sugimoto, Y. Watanabe, J.P. Korterik, N. Ikeda, N.F. van Hulst, K. Asakawa, L. Kuipers, Optics Express 14 (2006) 1658.
[8] A.Y. Petrov, M. Eich, Applied Physics Letters 85 (2004) 4866.
[9] M.D. Settle, R.J.P. Engelen, M. Salib, A. Michaeli, L. Kuipers, T.F. Krauss, Optics Express 15 (2007) 219.
[10] A.D. Falco, L. O'Faolain, T.F. Krauss., Applied Physics Letters 92 (2008) 083501.
[11] B. Wang, M.A. Dündar, R. Nötzel, F Karouta, Applied Physics Letters 97 (2010) 151105.
[12] S. Kubo, D. Mori, T Baba, Optics Express 32 (2007) 2981.
[13] L.H. Frandsen, A.V. Lavrinenko, J.F. Pefersen, P.I. Borel, Optics Express 14 (2006) 9444.
[14] S. Kubo, D. Mori, T. Baba, Optics Letters 32 (2007) 2981.
[15] N. Ozaki, Y. Kitagawa, Y. Takata, Optics Express 15 (2007) 7974.
[16] T.P. White, L.C. Botten, C.M. Sterke, K.B. Dossou, R.C. McPhedran, Optics Letters 33 (2008) 2644.
[17] J.T. Li, T.P. White, L. O'Faolain, A. Gomez-Iglesias, T.F. Krauss, Optics Express 16 (2008) 6227.
[18] F.C. Leng, W.Y. Liang, B. Liu, T.B. Wang, H.Z. Wang, Optics.Express 18 (2010) 5707.
[19] Y Hamachi, S. Kubo, T Baba, Optics Letters 34 (2009) 1072.
[20] M.E. Heidari, C. Grillet, C. Monat, B.J. Eggleton, Optics Express 17 (2009) 1628.
[21] J. Wu, Y.P. Li, C. Peng, Z.Y. Wang, Optics Communications 284 (2011) 2149.
[22] A. Casas Bedoya, P. Domachuk, C. Monat, C. Grillet, S. Tomljenovic-Hanic, E.C.Mägi, B. J. Eggleton. Proceedings of SPIE, 7949(2011), 794904.
[23] T. Baba, T. Kawasaki, H. Sasaki, J Adachi, D. Moriarge., Optics Express 16 (2008) 9245.
[24] S.C. Huang, M. Kato, E. Kuramochi, C.P. Lee, M. Notomi, Optics Express 15 (2007) 3543.
[25] K. Tian, W. Arora, S. Takahashi, J. Hong, G. Barbastathis, Physical Review B 80 (2009) 134305.
[26] G. Manzacca, H Habibian, K. Hinger, G. Cincotti, Photonics and Nanostructures—Fundamentals and Applications 7 (2009) 39–46.
[27] X. Chen, P Shum, J. Hu, Optics Communications 276 (2007) 93.
[28] K. Üstün, H. Kurt, Optics Express 18 (2010) 21155.
[29] S. Kocaman, X. Yang, J.F. McMillan, M.B. Yu, Applied Physics Letters 96 (2010) 221111.
[30] V.S.C. Manga Rao, S. Hughes, Optics Letters. 32 (2007) 304.
[31] J. Hou, H. Wu, D.S. Citrin, W. Mo, D. Gao, Z. Zhou, Optics Express 18 (2010) 10567.
[32] Y. Wan, Z. Cai, Q. Li, X.S. Zhao, Applied Physics A 102 (2011) 373.
[33] A. Têtu, M. Kristensen, L.H. Frandsen, A. Harpøth, P.I. Jensen, O. Sigmund, Optics Express 13 (2005) 8606.
[34] J. Liang, L. Ren, M. Yun, X. Wang, Applied Optics 50 (2011) 98.